IOP Publishing Journal of Geophysics and Engineering
J. Geophys. Eng. **13** (2016) 146–151 doi:10.1088/1742-2132/13/2/146

Reflection seismic waveform tomography of physical modelling data

Y Rao[1,2], Y Wang[2], Z D Zhang[3], Y C Ning[1], X H Chen[1] and J Y Li[1]

[1] State Key Laboratory of Petroleum Resources and Prospecting, China University of Petroleum (Beijing), Beijing, People's Republic of China
[2] Centre for Reservoir Geophysics, Department of Earth Science and Engineering, Imperial College London, London, UK
[3] Institute of Geology and Geophysics, Chinese Academy of Sciences, and University of Chinese Academy of Sciences, Beijing, People's Republic of China

E-mail: raoying@cup.edu.cn

Received 28 July 2015, revised 21 December 2015
Accepted for publication 18 January 2016
Published 8 March 2016

Abstract

Waveform tomography is commonly tested using numerically generated synthetic seismic data, before the method is applied to field seismic data. However, there are often noticeable differences between idealized synthetic data and real field data, and many factors in the field data, such as noise, irregular source/receiver geometry, affect the inversion solutions. For exploring the potential of reflection seismic waveform tomography, we presented a more realistic test than the synthetic data test, by applying it to physical modelling data, to reconstruct a laboratorial model with complex velocity variation. First, we provided a formulation of the perfectly matched layer absorbing boundary condition, associated with the second-order acoustic wave equation, in order to suppress artificial reflections from subsurface model boundaries in seismic waveform simulation and tomography. Then, we demonstrated the successful implementation of a layer-striping inversion scheme applicable to reflection seismic waveform tomography. Finally, we confirmed the effectiveness of frequency grouping, rather than a single frequency at each iteration, a strategy specifically for the frequency-domain waveform tomography.

Keywords: waveform tomography, perfectly matched layer, reflection seismic, full waveform inversion, layer striping scheme

(Some figures may appear in colour only in the online journal)

Introduction

Seismic waveform tomography, after its successful applications on direct waves in crosshole seismic (Wang and Rao 2006) and on refraction data with long source-receiver offsets (Pratt *et al* 1996, Brenders and Pratt 2007), has also been used to reflection seismic data (Wang and Rao 2009). The latter is the application to seismic data with a routine acquisition geometry adopted by seismic exploration. Since there are vast volumes of exploration seismic data exist, we do not need any extra investment to acquire data specifically for waveform tomography. Hence, reflection seismic waveform tomography has great potential in the industrial scale applications. While published literatures appear to focus on subsurface models consisting of sequentially layered structures with a modest velocity variation, here we attempts to investigate the capacity of reflection seismic waveform tomography in reconstructing a laboratorial model with a complex velocity variation.

In the research of waveform tomography, one often applies it first on numerically generated synthetic data, for exploring the potential, and then on field seismic data. However, there are often noticeable differences between idealized synthetic data and real field data, and many factors in field data, such as noise, irregular source/receiver geometry, can affect the inversion procedure. The final inversion result can only be verified by comparing the synthetic data, generated based on the reconstructed velocity model, with both well-log data and field seismic data (Kamei *et al* 2015). In this paper, we will

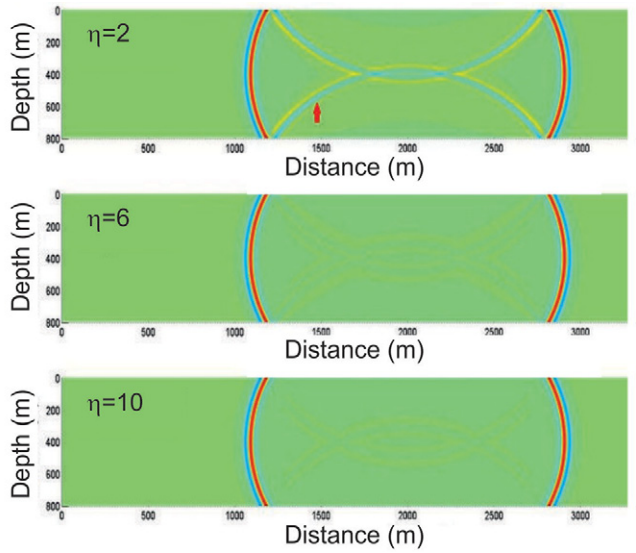

Figure 1. The snapshots when using the quadratic attenuation function. The attenuation coefficient η for each case is annotated in the image.

test waveform tomography on physical modelling data, and demonstrate its potential in recovering complex velocity variations. It is an intermediate test between synthetic and field data tests, but is more realistic than the synthetic test, for the application of reflection seismic waveform inversion.

In waveform tomography, the 'model' is limited by artificial boundaries, which generate unwanted reflections. One often set up an absorbing boundary condition (ABC), for simulating seismic wave propagation numerically in an infinite space. A commonly used ABC method is the paraxial approximation method (Clayton and Engquist 1977), which decomposes a two-way wave equation into two one-way equations and allows only the outward waves to pass a boundary and rejects the inward reflections from the boundary. The effectiveness of this paraxial approximation method strongly depends on the incidence angles at the boundary. Another commonly used ABC method is the Fourier damping layer method (Cerjan *et al* 1985), which uses a frequency-dependent damping function to attenuate the incidence waves within the damping layers around the computation area. This method directly acts on the discrete solution of wave equation, and hence suits to a frequency-domain wave simulation (Sochacki 1987, Hall and Wang 2009, Rao and Wang 2015). However, because of wave velocity variations in different directions, it is practically difficult to find an appropriate damping function.

In comparison to these two methods mentioned above, an ABC method with better performance would be the perfectly matched layer (PML) method (Berenger 1994), which attenuates waves gradually along with the increased distance in the boundary region. It is realized by a set of newly constructed equations for the attenuation zone. Classic PML methods work on either acoustic or elastic wave equations that are formulated as a first-order partial differential system in velocity and stress (Chew and Liu 1996, Hastings *et al* 1996, Liu and Tao 1997, Collino and Monk 1998, Qi and Geers 1998, Collino and Tsogka 2001, Basu and Chopra 2003). Komatitsch and Tromp (2003) proposed a PML formulation for the elastic wave equation written as a second-order system in displacement. In this paper, we will follow the work of Komatitsch and Tromp (2003) and formulate the PML condition associated with the second-order acoustic wave equation, and demonstrate the effectiveness of the quadratic attenuation function in this case.

While we check the capacity of waveform tomography in reconstructing a laboratorial physical model with complex velocity variations, we will demonstrate the implementation of a layer-striping inversion scheme, and confirm the effectiveness of frequency grouping, rather than a single frequency at each iteration. These two schemes are specifically applicable to the frequency-domain reflection seismic waveform tomography (Wang and Rao 2009).

Wave equation and the PML condition

In the waveform tomography, we use the following acoustic wave equation,

$$\frac{\omega^2}{v^2}U + \nabla^2 U = 0, \tag{1}$$

where ω is the angular frequency, v is the velocity, U is the acoustic wavefield, and ∇^2 is the Laplacian operator.

In the appendix, we derive the PML condition for this second-order acoustic wave equation. The wavefield U is decomposed into four parts.

$$U = P + Q + R + S. \tag{2}$$

The PML condition, working for the right-hand side boundary, for example, can be expressed as the following:

$$\begin{aligned}
&\frac{[d(x)+\mathrm{i}\omega]^2}{v^2}P - \frac{\partial^2 U}{\partial x^2} = 0\,,\\
&\frac{[d(x)+\mathrm{i}\omega]^3}{v^2}Q + \frac{\partial d(x)}{\partial x}\frac{\partial U}{\partial x} = 0\,,\\
&\frac{\mathrm{i}\omega[d(x)+\mathrm{i}\omega]}{v^2}R - 2\frac{\partial^2 U}{\partial x \partial z} = 0\,,\\
&\frac{\omega^2}{v^2}S + \frac{\partial^2 U}{\partial z^2} = 0\,.
\end{aligned} \tag{3}$$

Considering both the absorbing effect and computational efficiency, setting a proper attenuation function is critical in PML. If the attenuation is increased too slow, a thicker PML layer is required to absorb the wave energy, that would reduce the computational efficiency. If the attenuation function is increased too fast, internal reflections would be generated in the PML layer. We use a quadratic attenuation function as the following (Collino and Tsogka 2001):

$$d(n) = \eta\frac{v}{hN}\left(\frac{n-n_0}{N}\right)^2, \tag{4}$$

where η is a constant which controls the magnitude of the attenuation function, n_0 is the beginning position of PML layers, n is the position of incident waves, N is the thickness of PML layers, h is the space interval of finite-difference grids, and v is the wave velocity.

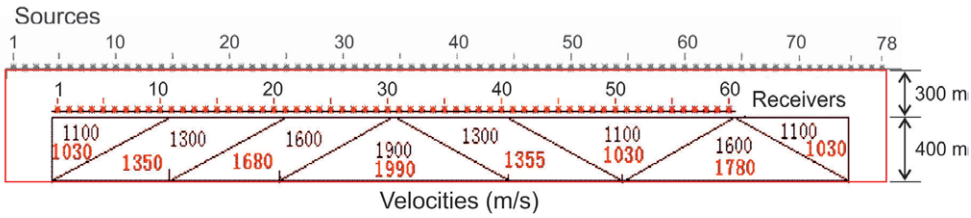

Figure 2. The physical model and the acquisition geometry. Within each velocity block, the velocity function varies linearly between two given values. There are 78 shots, and 60 receivers. The minimum source-receiver offset is 200 m, and the maximum source-receiver offset is 3150 m.

This quadratic attenuation function is increased along the distance $n - n_0$, and its derivative is also increasing. When using the quadratic attenuation function, it is easy to find an optimal attenuation coefficient which can both absorb the incidents and generate no internal reflections. As shown in figure 1, where the thickness of the PML is $N = 20$ cells, an optimal quadratic decay function with $\eta = 10$ can effectively attenuate the incident waves at the boundaries without visible internal reflections. The excellent attenuation performance of a PML condition and the modest thickness of the PML layer needed in finite-difference calculation are two advantages added to the effectiveness of the layer-striping inversion scheme, presented in the following sections.

Physical modelling seismic data

In the physical model, shown in figure 2, the dimensional is scaled properly to real world. The top water layer is 300 m in thickness, and the underneath is a 400 m target layer consisting of a series of velocity blocks, with relatively low velocity values but complex velocity variations. There are 78 source positions, each consisting of 60 traces. The minimum source-receiver offset of 200 m, and the maximum source-receiver offset of 3150 m.

Within each velocity block, the velocity function varies linearly along the depth between two listed velocity values. The lowest velocity within the entire model is 1030 m s^{-1}.

Figure 3 displays a shot gather of the laboratorial modelling data. The primary reflections from the top and the bottom horizons of the target velocity layer are marked by dashed red curves. The first-order water-layer multiple reflection from the top of the target velocity layer is marked by a dashed yellow curve. When we use a layer-striping inversion scheme, the prime object of the first layer inversion is the bottom of the water layer, which is the top horizon of the target velocity layer, and the prime data-fitting object in the second-layer inversion is the reflection from the bottom of the target velocity layer.

Figure 4(a) displays a common-offset (the minimum source-receiver offset) section of the raw seismic data. This profile, similar to field seismic data, shows primary reflections, multiple reflections, and data noise, etc. The current waveform tomography code uses the PML absorbing boundary condition at the free surface in wave simulation and the calculated wavefield does not include free surface multiples. Hence, multiple attenuation is a critical step in data pre-processing before

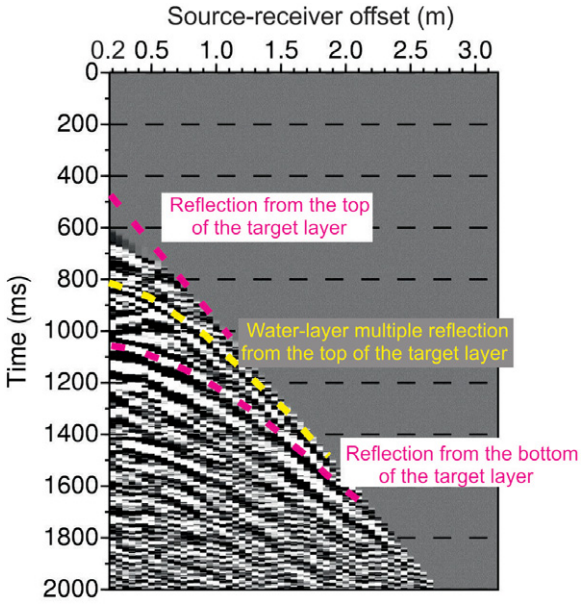

Figure 3. A shot gather of the laboratorial modelling data. The reflections from the top and the bottom of the target velocity layer are marked by dashed red curves. A water-layer multiple reflection from the top of the target velocity layer is marked by a dashed yellow curve.

waveform tomography (Wang and Rao 2009). We use the so-called multiple prediction through inversion (MPI) method (Wang 2004, 2007) to remove strong multiple reflections, so as to reduce the nonlinearity of the inverse problem, which is defined by data fitting.

Wavelets are extracted from all shots. The amplitude spectra of these wavelets (figure 4(b)) show the bandwidth of reflection data is 7−25 Hz. An average wavelet with proper amplitude magnitude is used in waveform tomography. The cell size in waveform tomography is 5 m, which satisfies the resolution requirement of four points per wavelength.

Reflection waveform tomography

Waveform tomography is a seismic inversion, with an objective function often defined by data misfit between synthetic and observed seismic data. This inverse problem is commonly solved iteratively, and at each iteration, the solution estimate is updated along the (negative) gradient of the objective function. For the gradient, it is a very time consuming task

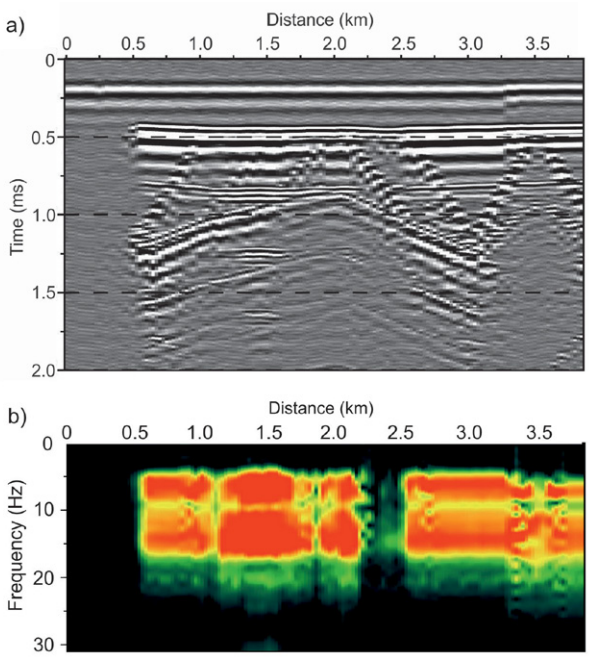

Figure 4. (a) The common-offset (the minimum offset) section of the raw seismic data set. (b) The amplitude spectrum of the wavelets.

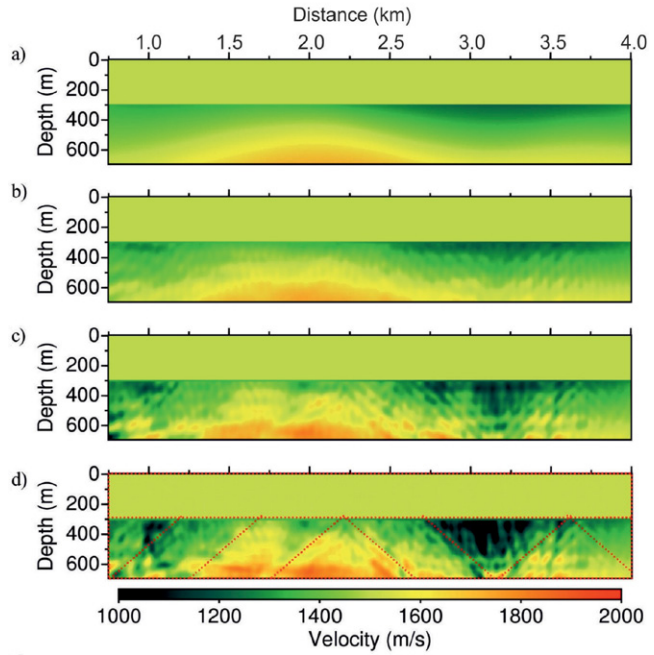

Figure 5. Waveform tomography. (a) The initial velocity model built by smoothed true velocity model. (b) The velocity model of waveform tomography using the first group of frequencies 7.0–7.8 Hz. (c) The velocity model of waveform tomography using frequencies in the range of 7.0–9.8 Hz. (d) The final velocity model obtained from the waveform tomography using all frequencies in the range of 7.0–24.8 Hz.

to numerically compute partial derivatives of the objective function, with respect to various model parameters. Tarantola (1984) proposed to calculate the gradient by a correlation of a forward wavefield and a residual back-propagated wavefield. It effectively runs forward calculation twice: One is standard forward wave simulation with a properly estimated wavelet, and another is same forward simulation but using data residual as the 'source waveform'. This scheme has significantly improved the efficiency of waveform tomography, or so-called full waveform inversion (Gauthier *et al* 1986, Pratt and Worthington 1990, Wang and Rao 2006, Rao *et al* 2006, Rao and Wang 2009).

In the physical model we study here, the first layer is a water layer, and we concentrate on reconstruction of the target layer of the model. We use a layer-stripping scheme for reflection seismic waveform tomography, presented in Wang and Rao (2009). The input shot gather to waveform inversion is a combination of an original shot record and a synthetic record: the top part is the synthetic data generated from the top water layer of the model, and the rest is the original seismic data. In the iterative solution update, the top portion of the model is kept unchanged, and the update is restricted to the bottom portion of the model.

The initial velocity model is built by smoothed true velocity model (figure 5(a)). In waveform tomography, a group of five frequencies is used simultaneously in each iterative inversion. The first group includes frequencies 7.0, 7.2, 7.4, 7.6 and 7.8 Hz, and the last group consists of 24.0, 24.2, 24.4, 24.6 and 24.8 Hz.

Compared with smooth start velocity model, a reconstructed velocity model, after using the first group of frequencies (figure 5(b)), shows some dipping events between 1000 and 1250 m and between 2750 and 3500 m in distance.

After using 3 groups of frequencies in ranges of 7.0–9.8 Hz, reconstructed velocity model (figure 5(c)), shows a downward-pointing triangle form between 2750 and 3650 m, a regular triangle form between 1750 and 2650 m, and parallelograms along the boundary of these two triangles between 1000 and 2150 m and 2250 and 3150 m.

After using all frequencies in the range of 7.0−24.8 Hz, reconstructed velocity model (figure 5(d)) shows sharper boundaries of velocity blocks. The lower velocity area, with parallelogram shape, between 1250 and 1750 m, has been recovered with velocity value equal to 1300−1350 m s^{-1}, and the lower velocity area, with downward-pointing triangle shape, between 2750 and 3650 m, has been recovered with velocity value equal to 1100−1030 m s^{-1}. At the right hand side of this triangle, the regular triangle is with velocity of 1600−1780 m s^{-1} as true physical model.

In summary, the reconstructed velocity model shows clearly the sequence of these velocity blocks: right-angle triangle, parallelogram, parallelogram, regular triangle, parallelogram, downward-pointing triangle, regular triangle, right-angle triangle.

Conclusions

This paper has tested the capacity of reflection seismic waveform tomography to reconstruct a laboratorial model with complex velocity variations. The test on physical modelling data in this paper would act as a bridge between synthetic tests and real data tests, for the application of reflection seismic waveform inversion.

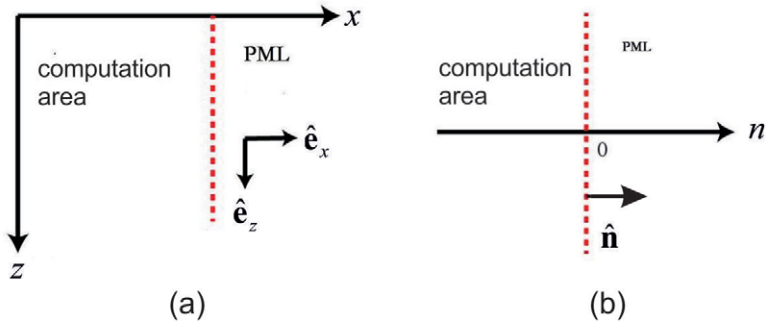

Figure 6. (a) The axes for converting a vector equation to a scalar equation, where $\hat{\mathbf{e}}_x$ and $\hat{\mathbf{e}}_z$ are the unit vectors in x and z direction, respectively. (b) Schematic diagram of computation domain and PML boundary, where n is a coordinate axis perpendicular to the border, and the $\hat{\mathbf{n}}$ is its normal unit vector normal to the border.

For suppressing the artificial reflections from the artificial boundaries and numerically simulating seismic wave propagation in an infinite space, this paper has provided a detailed derivation of the PML boundary condition, associated with the second-order acoustic wave equation. It has also demonstrated that the quadratic attenuation function is suitable for the PML boundary condition of second-order acoustic wave equation.

While examining the capacity of waveform tomography in reconstruct the laboratory model, this paper has confirmed the effectiveness of the layer-striping inversion scheme and a scheme of grouping frequencies in each iteration, presented in reflection seismic waveform tomography.

Acknowledgments

We are grateful to National Natural Science Foundation of China (grant nos. 41474111 and U1262207) and the sponsors of the Centre for Reservoir Geophysics, Imperial College London, for supporting this research.

Appendix. The PML condition for the second-order acoustic wave equation

In wave equation (1), the acoustic wavefield U is a scalar. However, in order to facilitate the derivation of the PML condition, we partition this scalar quantity into two orthogonal components, in 2D case, and represent it as a vector,

$$\mathbf{U} = U_x\hat{\mathbf{e}}_x + U_z\hat{\mathbf{e}}_z \tag{A.1}$$

where $\hat{\mathbf{e}}_x$ and $\hat{\mathbf{e}}_z$ are the unit vectors in the x and z direction, respectively (figure 6), and U_x and U_z are the projected wavefield components. Using vectorization, the frequency-domain acoustic wave equation can be expressed as

$$\frac{\omega^2}{v^2}\mathbf{U} + \nabla^2\mathbf{U} = 0. \tag{A.2}$$

By doing this vectorization, we can derive the PML condition from equation (A.2), following Komatitsch and Tromp (2003).

The partial derivatives, with respect to x and z, respectively, can also form a vector

$$\nabla = \frac{\partial}{\partial x}\hat{\mathbf{e}}_x + \frac{\partial}{\partial z}\hat{\mathbf{e}}_z. \tag{A.3}$$

It follows that the Laplacian operator is the inner product of two vectors, $\nabla^2 = \nabla\cdot\nabla$.

Following Komatitsch and Tromp (2003), let us define a unit vector $\hat{\mathbf{n}}$ which is perpendicular to the border separating the computational area and the PML boundary (figure 6(a)). The Laplacian operator can be decomposed into two components:

$$\nabla = \hat{\mathbf{n}}\partial_n + \nabla^{\parallel}, \tag{A.4}$$

where $\partial_n = \hat{\mathbf{n}}\cdot\nabla$, hence $\hat{\mathbf{n}}\partial_n$ is the component perpendicular to the border, and $\nabla^{\parallel}$ is the component in the surface parallel to the border. The latter can be expressed as $\nabla^{\parallel} = (\mathbf{I} - \hat{\mathbf{n}}\hat{\mathbf{n}})\cdot\nabla$, where $\mathbf{I}$ is a 2×2 identical matrix for 2D case, and $(\mathbf{I} - \hat{\mathbf{n}}\hat{\mathbf{n}})$ is the projection operator on to the surface with normal $\hat{\mathbf{n}}$. Therefore, the second-order wave equation (A.2) can be rewritten as

$$\frac{\omega^2}{v^2}\mathbf{U} + (\hat{\mathbf{n}}\partial_n\cdot\hat{\mathbf{n}}\partial_n + \hat{\mathbf{n}}\partial_n\cdot\nabla^{\parallel} + \nabla^{\parallel}\cdot\hat{\mathbf{n}}\partial_n + \nabla^{\parallel}\cdot\nabla^{\parallel})\mathbf{U} = 0. \tag{A.5}$$

Within the PML absorbing boundary, the coordinate n is replaced with a complex coordinates $\tilde{n}$, defined by

$$\tilde{n}(n) = n + \frac{1}{\mathrm{i}\omega}\int_0^n d(\ell)\,\mathrm{d}\ell, \tag{A.6}$$

where i is the imaginary symbol, $d(\ell)\geqslant 0$ is an attenuation function, and ℓ is the distance along the attenuation direction, measured from the border. Changing variable $n\to\tilde{n}$ is equivalently to the following change to partial differential:

$$\partial\to\frac{1}{s_n}\partial_n, \tag{A.7}$$

where s_n is a complex stretching factor. Thus equation (A.5) can be rewritten as

$$\frac{\omega^2}{v^2}\mathbf{U} + \left[\frac{1}{s_n^2}\hat{\mathbf{n}}\partial_n\cdot\hat{\mathbf{n}}\partial_n + \frac{1}{s_n}\partial_n\left(\frac{1}{s_n}\right)\hat{\mathbf{n}}\cdot\hat{\mathbf{n}}\partial_n + \frac{1}{s_n}(\hat{\mathbf{n}}\partial_n\cdot\nabla^{\parallel} + \nabla^{\parallel}\cdot\hat{\mathbf{n}}\partial_n) + \nabla^{\parallel}\cdot\nabla^{\parallel}\right]\mathbf{U} = 0. \tag{A.8}$$

In equations (A.7) and (A.8), the complex stretching factor is defined by

$$s_n \equiv \frac{\partial \tilde{n}}{\partial n} = 1 + \frac{d(n)}{\mathrm{i}\omega}, \tag{A.9}$$

derived from expression (A.6).

Decomposing wavefield $\mathbf{U}$ into four parts,

$$\mathbf{U} = \mathbf{P} + \mathbf{Q} + \mathbf{R} + \mathbf{S}, \tag{A.10}$$

each of which corresponds to a term inside the square brackets of equation (A.8), respectively, we have the following system of equations:

$$\begin{aligned}
\frac{\omega^2}{v^2}\mathbf{P} + \frac{1}{s_n^2}\hat{\mathbf{n}}\partial_n \cdot \hat{\mathbf{n}}\partial_n \mathbf{U} = 0, \\
\frac{\omega^2}{v^2}\mathbf{Q} + \frac{1}{s_n}\partial_n\left(\frac{1}{s_n}\right)\hat{\mathbf{n}} \cdot \hat{\mathbf{n}}\partial_n \mathbf{U} = 0\,, \\
\frac{\omega^2}{v^2}\mathbf{R} + \frac{1}{s_n}(\hat{\mathbf{n}}\partial_n \cdot \nabla^{\parallel} + \nabla^{\parallel} \cdot \hat{\mathbf{n}}\partial_n)\mathbf{U} = 0\,, \\
\frac{\omega^2}{v^2}\mathbf{S} + \nabla^{\parallel} \cdot \nabla^{\parallel}\mathbf{U} = 0\,.
\end{aligned} \tag{A.11}$$

Based on equation (A.9), a derivation of the stretching factor with respect to the variable n is

$$\partial_n\left(\frac{1}{s_n}\right) = -\frac{\mathrm{i}\omega}{[\mathrm{i}\omega + d(n)]^2}\frac{\partial d(n)}{\partial n}. \tag{A.12}$$

Equation (A.11) becomes

$$\begin{aligned}
\frac{[\mathrm{i}\omega + d(n)]^2}{v^2}\mathbf{P} - \hat{\mathbf{n}}\partial_n \cdot \hat{\mathbf{n}}\partial_n \mathbf{U} = 0\,, \\
\frac{[\mathrm{i}\omega + d(n)]^3}{v^2}\mathbf{Q} + \frac{\partial d(n)}{\partial n}\hat{\mathbf{n}} \cdot \hat{\mathbf{n}}\partial_n \mathbf{U} = 0\,, \\
\frac{\mathrm{i}\omega[\mathrm{i}\omega + d(n)]}{v^2}\mathbf{R} - (\hat{\mathbf{n}}\partial_n \cdot \nabla^{\parallel} + \nabla^{\parallel} \cdot \hat{\mathbf{n}}\partial_n)\mathbf{U} = 0\,, \\
\frac{\omega^2}{v^2}\mathbf{S} + \nabla^{\parallel} \cdot \nabla^{\parallel}\mathbf{U} = 0\,.
\end{aligned} \tag{A.13}$$

Since the acoustic wavefield is a scalar, the associated PML condition for the right-hand side boundary, where $\hat{\mathbf{n}} = \hat{\mathbf{e}}_x$, can be expressed as a system of scalar equations, presented in main text as equations (2) and (3).

Note that the PML boundary condition, in the frequency-domain, can be derived by second-order wave equation straightforwardly without wavefield separation (Rao and Wang 2013). However, an advantage of the vectorised form in equation (A.13) is that it can be applied to any boundary with a normal direction $\hat{\mathbf{n}}$ not necessarily the same as the x or z directions.

References

Basu U and Chopra A K 2003 Perfectly matched layers for time-harmonic elastodynamics of unbounded domains: theory and finite-element implementation *Comput. Methods Appl. Mech. Eng.* **192** 1337–75

Berenger J P 1994 A perfectly matched layer for the absorption of electromagnetic waves *J. Comput. Phys.* **114** 185–200

Brenders A J and Pratt R G 2007 Efficient waveform tomography for lithospheric imaging: implications for realistic, two-dimensional acquisition geometries and low-frequency data *Geophys. J. Int.* **168** 133–51

Cerjan C, Kosloff D, Kosloff R and Reshef M 1985 A nonreflecting boundary condition for discrete acoustic and elastic wave equations *Geophysics* **50** 705–8

Chew W C and Liu Q 1996 Perfectly matched layers for elastodynamics: a new absorbing boundary condition *J. Comput. Acoust.* **4** 341–59

Clayton R and Engquist B 1977 Absorbing boundary conditions for acoustic and elastic wave equations *Bull. Seismol. Soc. Am.* **67** 1529–40

Collino F and Monk P 1998 Optimizing the perfectly matched layer *Comput. Methods Appl. Mech. Eng.* **164** 157–71

Collino F and Tsogka C 2001 Application of the perfectly matched absorbing layer model to the linear elastodynamic problem in anisotropic heterogeneous media *Geophysics* **66** 294–307

Gauthier O, Virieux J and Tarantola A 1986 Two-dimensional non-linear inversion of seismic waveforms: numerical results *Geophysics* **51** 1387–403

Hall F and Wang Y 2009 Elastic wave modelling by an integrated finite difference method *Geophys. J. Int.* **177** 104–14

Hastings F D, Schneider J B and Broschat S L 1996 Application of the perfectly matched layer (PML) absorbing boundary condition to elastic wave propagation *J. Acoust. Soc. Am.* **100** 3061–9

Kamei R, Miyoshi T, Pratt R G, Takanashi M and Masaya S 2015 Application of waveform tomography to a crooked-line 2D land seismic data set *Geophysics* **80** B115–29

Komatitsch D and Tromp J 2003 A perfectly matched layer absorbing boundary condition for the second-order seismic wave equation *Geophys. J. Int.* **154** 146–53

Liu Q and Tao J 1997 The perfectly matched layer for acoustic waves in absorptive media *J. Acoust. Soc. Am.* **102** 2072–82

Pratt R G and Worthington M H 1990 Inverse theory applied to multi-source crosshole tomography, part I: acoustic wave equation method *Geophys. Prospect.* **38** 287–310

Pratt R G, Song Z M, Williamson P and Warner M 1996 Two-dimensional velocity models from wide-angle seismic data by wavefield inversion *Geophys. J. Int.* **124** 323–40

Qi Q and Geers T L 1998 Evaluation of the perfectly matched layer for computational acoustics *J. Comput. Phys.* **139** 166–83

Rao Y, Wang Y and Morgan J 2006 Crosshole seismic waveform tomography—II. Resolution analysis *Geophys. J. Int.* **166** 1237–48

Rao Y and Wang Y 2009 Fracture effects in seismic attenuation images reconstructed by waveform tomography *Geophysics* **74** R25–34

Rao Y and Wang Y 2013 Seismic waveform simulation with pseudo-orthogonal grids for irregular topographic models *Geophys. J. Int.* **194** 1778–88

Rao Y and Wang Y 2015 Seismic attenuation in fractured media *J. Geophys. Eng.* **12** 26–32

Sochacki J, Kubichek R, George J, Fletcher W R and Smithson S 1987 Absorbing boundary conditions and surface waves *Geophysics* **52** 60–71

Tarantola A 1984 Inversion of seismic reflection data in the acoustic approximation *Geophysics* **49** 1259–66

Wang Y 2004 Multiple prediction through inversion: a fully data-driven concept for surface-related multiple attenuation *Geophysics* **69** 547–53

Wang Y and Rao Y 2006 Crosshole seismic waveform tomography, I: strategy for real data application *Geophys. J. Int.* **166** 1224–36

Wang Y 2007 Multiple prediction through inversion: Theoretical advancements and real data application *Geophysics* **72** V33–9

Wang Y and Rao Y 2009 Reflection seismic waveform tomography *J. Geophys. Res.* **114** B03304